ELSEVIER

Contents lists available at ScienceDirect

Journal of Alloys and Compounds

journal homepage: www.elsevier.com/locate/jalcom



Fe-based metallic glass ribbons as dual electrodes for ultrasonic cavitation-enhanced electro-Fenton degradation of ofloxacin

Yu Zhang ^a, Zhenxuan Zhang ^{a,*} ^o, Kunheng Zou ^a, Mengting Yang ^b, Wenqing Ruan ^a, Changyong Liu ^a, Xiong Liang ^{a,*}, Jiang Ma ^{a,*}

ARTICLE INFO

Keywords: Metallic glass Ultrasonic cavitation Advanced oxidation processes Electro-Fenton Ofloxacin

ABSTRACT

Electrochemical degradation holds significant promise for wastewater treatment. This study introduces an ultrasonic cavitation-enhanced electrochemical degradation system that employs Fe-Si-B metallic glass ribbons as both cathodic and anodic materials for the degradation of ofloxacin (OFL) in wastewater. Under acidic conditions (pH = 3) with a 25 mA applied current, the system achieves a good degradation efficiency (98.4 %) for 25 mg/L OFL within 30 min. The OFL removal efficiency increases with rising current. Anodic oxidation induces the formation of cluster-like oxidized structures on the ribbon surface, which enhances the hydrophilicity of the electrodes. Ultrasonication further promotes the development of these clustered morphologies and improves the electrodes' hydrophilicity. Moreover, ultrasonic assistance boosts degradation performance, particularly during the initial reaction stage by increasing the removal efficiency from 33.4 % to 61.5 % within the first 15 min. It also enhances the mineralization efficiency 3-fold (from 12.1 % to 36.3 %) and raises the reaction rate constant by 1.52 times (from $0.02361 \, \text{min}^{-1}$ to $0.03587 \, \text{min}^{-1}$). Hydroxyl radicals and hydrogen radicals are identified as the dominant reactive species involved in the degradation mechanism. After 10 reuse cycles, the Fe-based amorphous ribbon maintained a degradation rate of nearly 90 %, highlighting its remarkable stability. This work provides an efficient and robust strategy for antibiotic wastewater treatment and highlights the potential of amorphous materials for advanced oxidation processes.

1. Introduction

Antibiotics, as a type of antibacterial drug, have played a crucial role in the development history of human society. Hundreds of thousands of tons of antibiotics are used in clinical medicine and aquaculture every year. However, in actual production, there are generally high levels of antibiotic residues in the wastewater from the pharmaceutical industry, medical institutions, and aquaculture industry [1,2]. The residues of these antibiotics and their metabolites in water bodies are bound to lead to the disruption of the original ecological balance of the water environment. The total amount of antibiotics emissions in the Yangtze River basin exceeded 1600 tons per year between 2013 and 2021 [3]. The accumulation of these antibiotics can cause great risk to human health [4]. The efficient and clean treatment of antibiotic wastewater has emerged as a critical issue concerning ecology, economy, and human health.

The electro-Fenton (EF) process is an effective advanced oxidation

process, which is cleaner and easier compared with other degradation techniques. Compared with other processes, electro-Fenton does not require the addition of extra oxidants such as H_2O_2 , avoiding the risks in the transportation and storage of oxidants. Instead, it generates oxidants in-situ, featuring a cleaner and safer characteristic. In recent years, EF has gained considerable attention due to its remarkable degradation performance, simplicity and low cost in wastewater treatment [5]. Electro-Fenton process has demonstrated considerable potential in treating dye wastewater, medical wastewater and industrial wastewater [6,7].

Ultrasound, as an energy stimulus, has been confirmed to promote chemical reactions, particularly enhancing the degradation of complex matrices, such as pharmaceutical compounds and personal care products [8,9]. Due to the presence of cavitation effect, ultrasound can promote mass transfer and enhance reaction rates. The tiny bubbles generated in the reaction by ultrasonic crack after reaching a certain size, releasing local high temperature and pressure, which enhances the

E-mail addresses: zxzhang@szu.edu.cn (Z. Zhang), xliang@szu.edu.cn (X. Liang), majiang@szu.edu.cn (J. Ma).

^a College of Mechatronics and Control Engineering, Shenzhen University, Shenzhen 518060, China

^b College of Chemistry and Environmental Engineering, Shenzhen University, Shenzhen 518060, PR China

^{*} Corresponding authors.

mass transfer efficiency. Additionally, ultrasound facilitates the generation of hydroxyl radicals and other reactive species [10], which is significant for contaminants degradation. However, ultrasound still faces the issues of narrow adaptability and low energy utilization efficiency. Combining it with other advanced oxidation processes (AOPs) can effectively address these problems [11].

Electrode materials play a vital role in electrochemical reactions. Choosing an appropriate electrode material is not only beneficial to increasing the reaction rate, but also can reduce the leaching rate of the materials, expand the reaction scope, and improve the reaction adaptability [12]. For wastewater treatment, most current research primarily focuses on composite electrode materials and noble metal electrode materials, such as Pt, Pd, etc. [13,14]. Although noble metal electrodes exhibit excellent catalytic performance, their high cost restricts large-scale application. There is an urgent need to explore more cost-effective electrode materials that can efficiently treat wastewater at a lower cost [15]. The combination of different advanced oxidation processes, such as electrocatalysis, ozonation catalysis, ultrasonic catalysis, and photocatalysis, can bring new improvements to degradation processes [16].

Transition metals have emerged as a critical source of catalysts in AOPs due to their notable catalytic activity and structural stability [17]. Among them, Fe-based materials stand out for their alloy design versatility, allowing tailored compositions via strategic doping of metallic elements [18,19]. This flexibility enables functional applications in heterogeneous catalysis, with enhanced performance attributed to d-orbital electron accessibility that facilitates redox electron transfer. Furthermore, compared with other transition metals, iron-based materials stand out for their advantages of low cost, easy availability, and strong environmental adaptability [20,21]. Metallic glass materials, due to their long-range structural disorder and metastable energy state, exhibit excellent physical properties and have been widely used in the field of catalysis [22]. Amorphous alloys with different compositions have been used as electrodes in electrocatalytic reactions and batteries, achieving remarkable results [23,24]. Based on this, the selection of iron-based amorphous alloys as catalysts for the Fenton reaction is beneficial for further enhancing the catalytic performance of the system. They have been widely applied in various fields such as magnetic materials, transformers, and catalytic reactions [25,26]. However, their use as electrode materials in organic wastewater degradation has not been extensively studied.

In this study, the Fe₇₈Si₉B₁₃ metallic glass (Fe-MG) was selected as the electrode material to degrade antibiotics ofloxacin (OFL). OFL is one of the most widely used antibiotics [27]. Even low concentrations of OFL residues can affect biological reproduction and ecological balance. In recent years, researchers have conducted extensive studies on the degradation of OFL using AOPs [28,29]. While metallic glasses have been used in catalytic and electrochemical wastewater treatment particularly for dye degradation [30], their application antibiotic-laden effluents and the role of ultrasound remain under-explored. Here, we employ Fe-based metallic glass ribbons as electrodes and systematically elucidate ultrasound-electrode synergy in antibiotic degradation, thereby extending the application scope and providing mechanistic insight. The main objectives of the present study are to investigate the degradation efficiency and reaction mechanism of OFL-containing antibiotic wastewater in an electrochemical system using Fe-MG ribbons as electrodes, and to explore the enhancement effect of ultrasonic cavitation on the degradation process. The influences of reaction factors such as pH value, pollutant concentration and electrolyte concentration on the degradation were also investigated. The surface morphological and elemental valence state variations of Fe-MG ribbons before and after the reaction were characterized. The primary reactive species involved in the reaction were also identified. The results of this study may open up a new approach for the application of amorphous materials in wastewater treatment.

2. Materials and methods

2.1. Materials

The $Fe_{78}Si_9B_{13}$ metallic glass ribbon, was prepared in an arc furnace through the rapid cooling method. The preparation process is roughly as follows: Weigh the corresponding masses of Fe, Si, and B elements required according to the pre-calculation. All the elements used in the process of preparing the material in this study are of 99.9 % purity. Subsequently, using argon as the protective gas, the elemental substances are placed in the arc furnace, and an arc is struck and smelted repeatedly within the current range of 120 A to 200 A to obtain a homogeneous Fe-Si-B ingot. Then, the ingot is placed in a test tube, and a homogeneous Fe-MG ribbon is obtained through single-roll melting in a ribbon casting machine. An X-ray diffractometer is used to confirm its amorphous composition. The obtained $Fe_{78}Si_9B_{13}$ is vacuum annealed at a temperature of 873.15 K for 1 h. After cooling, the $Fe_{78}Si_9B_{13}$ crystallized ribbon can be obtained.

Ofloxacin (OFL, 98 %), and sodium sulfate (Na_2SO_4 , 99 %) were purchased from Macklin (Shanghai, China). Ultrapure water was used throughout the whole catalytic degradation experiments for dissolution.

2.2. Experimental setup

The electrochemical (EC) degradation experiments were executed within a 250 mL beaker. A magnetic stirrer operating at 400 r/min was utilized to ensure homogeneous mixing of the solution. Two Fe-MG ribbons, each measuring 7 cm in length and 1 cm in width, were respectively designated as the cathode and anode. These electrodes were arranged in a parallel configuration, and the inter electrode distance was maintained at a constant 3 cm during the experimental procedures. The electrodes were electrically connected to a direct current power supply to achieve a precisely specified applied current. The degradation solution (OFL) was prepared with a concentration of 25 mg/L. Na₂SO₄ (0.05 mol/L) was introduced as an electrolyte to enhance the solution's electrical conductivity. When investigating the degradation behavior under different pH values, pre-diluted dilute sulfuric acid and sodium hydroxide solutions were employed to modulate the solution's pH. The pH value of the solution was accurately measured using a pH meter (FE-28, Mettler).

The ultrasound-electrochemical degradation experiments were conducted within a reaction flask with an inner diameter of 110 mm and an approximate height of 150 mm. An ultrasonic generator with an output frequency of 20 kHz was used to generate ultrasonic waves. The ultrasonic probe was positioned 2 cm above the bottom of the solution to ensure uniform cavitation distribution.

At regular time intervals during the experiment, a fixed-volume aliquot of the reaction solution was withdrawn from the container and measured for fluorescence intensity using a fluorescence spectrophotometer (FL8500, PerkinElmer). The wavelength range for the measurement was set between 260 and 420 nm. Given that the fluorescence intensity of the solution is directly proportional to the concentration of organic compounds, the degradation efficiency of the reaction can be effectively characterized by fluctuations in fluorescence intensity. All experiments were performed with three parallel samples (n = 3) and error bars represent the standard deviation calculated from the three parallel samples.

Total organic carbon (TOC) analysis was employed to assess the changes in the organic carbon content within the solution during the reaction progression. After sample withdrawal, the solution was filtered through a $0.22\,\mu m$ polyether sulfone (PES) membrane and subsequently analyzed using a Shimadzu organic carbon analyzer (TOC-L). This demonstrates the mineralization efficiency of the ultrasound-electrochemical composite system towards organic pollutants.

The OFL metabolites generated during catalysis reaction were measured by UPLC-MS/MS on a UPLC (Acquity I-class, Waters) coupled

with electrospray ionization (ESI)-MS/MS (Xevo TQ-S micro, Waters) system. An HSS T3 (1.8 $\mu m, 2.1 \times 100$ mm, Waters) column was selected for the UPLC separation and the column temperature was set at 35 $^{\circ}$ C. The injection volume was 5 μL . The mobile phase was water and methanol at a flow rate of 0.40 mL/min. The mobile phase gradient was initially set to 5 % methanol and 95 % water, changed linearly to 90 % methanol and 10 % water in the first 8 min, and then rapidly returned to 5 % methanol and 95 % water in 0.1 min and then held for additional 2.9 min to re-equilibrate.

2.3. Characterization of metal materials

X-ray diffractometer (XRD, Rigaku MiniFlex600) was utilized to test the structural characteristics of the $Fe_{78}Si_9B_{13}$ amorphous ribbons, the crystallized ribbons, and the surface of the iron foil before and after the reaction. X-ray photoelectron spectroscopy (XPS, Thermo Scientific K-Alpha) was used for elements and valence states identification. Scanning electron microscope (SEM, ZEISS Sigma 300) equipped with an energy-dispersive spectrometer (EDS) was employed to observe the alterations in the surface morphology and elemental distribution of the ribbons subsequent to the degradation reaction

2.4. Analytical procedures

Fluorescence spectrophotometry (PerkinElmer FL8500) was used to determine the concentration of OFL in the solution. Synchronous fluorescence method can narrow the spectral band and improve the sensitivity of the test with optimized scanning range of 260 nm to 420 nm, and the optimal $\Delta\lambda$ was selected as 130 nm after comparison [31]. Based on the variation of the intensities of the fluorescence characteristic peaks of solution, the change of the solution concentration can be obtained. Thus, the removal efficiency of OFL can be calculated by Eq. (1):

$$\eta = \frac{C_0 - C_t}{C_0} \quad * \quad 100\% \tag{1}$$

The reaction follows a pseudo-first-order kinetic equation, and its reaction constant can be expressed as followed in Eq. (2):

$$-\frac{dC}{dt} = kC \tag{2}$$

Accordingly, by combining with Eq. (1), it can be concluded that the calculation formula of the reaction constant k as shown in Eq. (3):

$$\ln\left(\frac{C_0}{C_t}\right) = kt$$
(3)

3. Results and discussion

3.1. Degradation performance of US/EC system

3.1.1. Degradation performance under different applied current

Electrochemical degradation experiments were conducted to investigate the degradation efficiency of OFL-containing wastewater using Fe-MG as electrodes. The standard experimental conditions were set as follows: $25\ mg/L$ of OFL, $0.05\ mol/L$ of Na_2SO_4 , and a solution pH of 3. As illustrated in Fig. 2a, the concentration of the OFL solution demonstrates a continuous decrease over time under a $15\ mA$ applied current. Only $9.4\ \%$ of the initial OFL concentration remains in the solution within $45\ min$ under $15\ mA$. This result confirms the effectiveness of the electrochemical degradation system using Fe-MG ribbons as electrodes.

The applied current represents a critical parameter in electrochemical systems. To further clarify the effect of current on the degradation process, a series of experiments with different applied current values (5 mA, 15 mA, 25 mA) were conducted. As depicted in Fig. 2d, the degradation efficiency of OFL demonstrates a steady increase with rising current intensity. A slight difference in degradation efficiency is

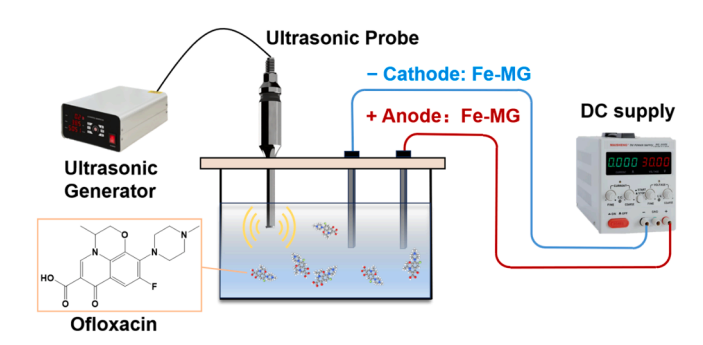


Fig. 1. Diagram of experimental setup for ultrasonic cavitation-enhanced electro-Fenton degradation of ofloxacin.

observed as the current increases from 5 mA to 15 mA. Notably, when the current is raised to 25 mA, the proportion of degraded OFL within the first 15 min surges from 31.8 % (at 5 mA) to 80.6 %, indicating that higher current intensities considerably enhance OFL degradation. The corresponding kinetic constants was also increased by 1.9 times, from 0.02361 $\rm min^{-1}$ (15 mA) to 0.04497 $\rm min^{-1}$ (25 mA). A previous study using a Cu-Fe composite oxide catalyst to activate persulfate for OFL degradation required 30 min to achieve 90 % removal of 10 mg/L OFL. In sharp contrast, under a similar time frame (30 min), the Fe-MG system achieved complete degradation of OFL at a significantly higher initial concentration of 25 mg/L. This comparison clearly underscores the superior degradation rate and efficiency of our proposed system [32].

The magnitude of the applied current is crucial for multiple aspects of electrochemical reactions. As the current increases, the electric field strength at the electrode surface enhances, leading to a continuous acceleration of electron transfer rate. According to Faraday's law, the increase of current intensity promotes the cathodic release of iron ions [33], which is critical for the formation of •OH. However, excessively high current not only increases reaction energy consumption but also favors the generation of hydrogen peroxide radicals (•OOH) over •OH. Since •OOH exhibits weaker oxidizing properties, this hinders catalytic reactions [34]. Conversely, insufficient current may fail to generate adequate reactive species such as free radicals and H2O2, thereby impeding the catalytic process. The degradation efficiency of the system using Fe-MG as the electrode exhibits a distinct advantage compared with those of systems based on other traditional materials or novel composite materials. Under optimal conditions, when Bio-FeMnOx was used as the cathode material at a current density of 50 mA/cm², it took nearly 180 min to completely degrade 20 mg/L OFL [35]. Cao et al. developed a self-adsorptive system for ofloxacin (OFL) degradation. The incorporation of an aeration device enhances the recycling efficiency of reactive substances. The whole process took 105 min to completely degrade 25 mg/L of OFL at a pH of 3 [36]. In summary, compared with other systems, the use of Fe-MG as electrodes enables more efficient degradation of OFL. Increasing the current within a reasonable range facilitates electron accumulation, thereby further promoting the degradation of OFL.

3.1.2. Degradation performance under different ultrasonic power

Following the clarification of the current's impact on the reaction, ultrasound was introduced into the reaction system to explore its potential for promoting the electrochemical degradation process. Experiments were performed under the conditions of pH= 3, 25 mg/L OFL, 0.05 mol/L Na₂SO₄, and a constant applied current of 15 mA, with different ultrasonic power levels applied (200 W, 280 W, 360 W). As illustrated in Fig. 2b, introducing 280 W ultrasound into the system under a 15 mA current resulted in an OFL degradation efficiency of 50.2 % after 15 min of reaction. In comparison, the degradation efficiency without ultrasound was only 33.4 %, demonstrating an increase in reaction efficiency by ultrasound. Fig. 3c reveals that the application

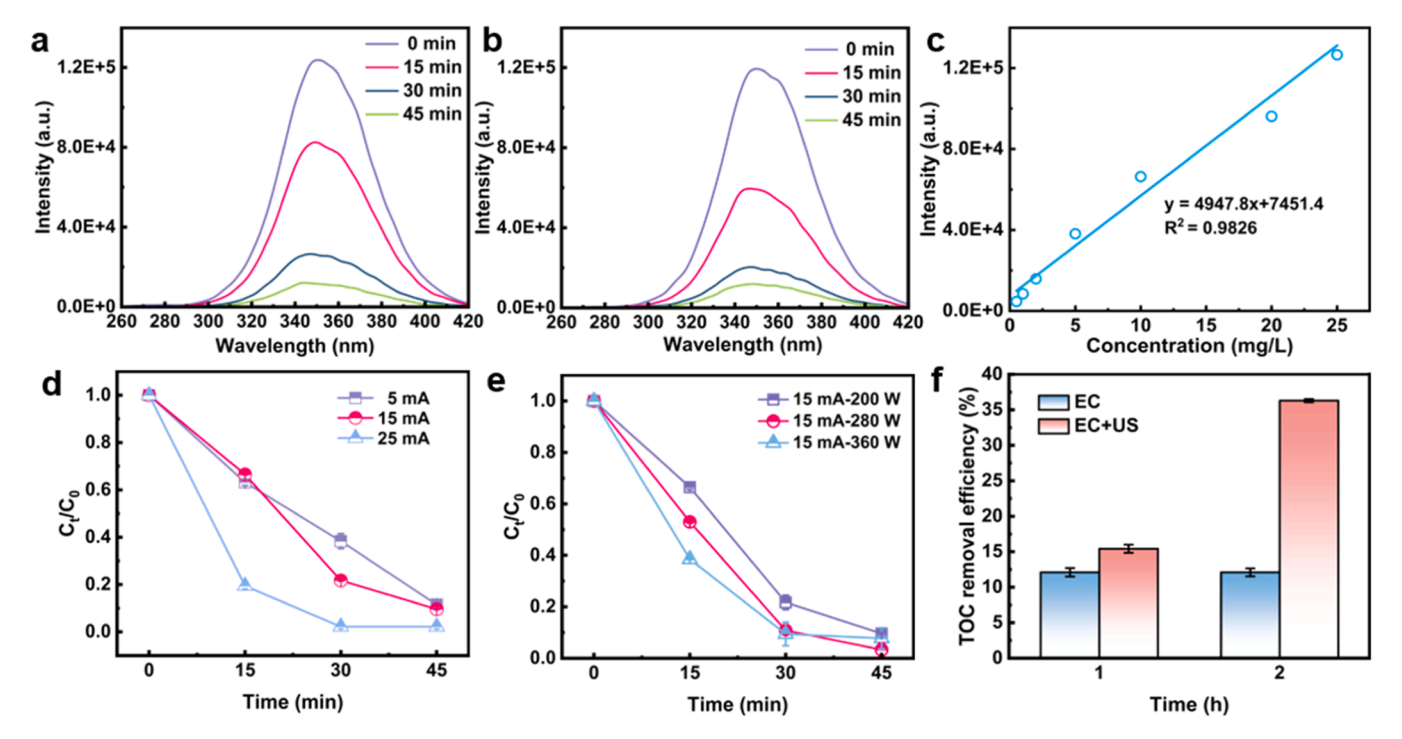


Fig. 2. (a) Fluorescence spectrum of OFL degradation process under applied current (15 mA), (b) Fluorescence spectrum of OFL degradation process under applied current (15 mA) and ultrasound loading (280 W), (c) standard curve for the quantification of OFL, (d) degradation efficiency of OFL under different applied current, (e) degradation efficiency of OFL under different ultrasound loading power, (f) TOC removal efficiency of OFL with and without ultrasound loading. Conditions: $[Na_2SO_4] = 0.05 \text{ mol/L}$, pH = 3, [OFL] = 25 mg/L.

of ultrasound led to a 1.52-fold increase in k (from 0.02361 min⁻¹ to 0.03587 min⁻¹). Such an efficiency improvement exhibits a distinct advantage compared with other ultrasonic-electrochemical degradation systems. Ritesh et al. used Ti/RuO2 as the anode and stainless steel as the cathode, and degraded a 20 mg/L OFL solution in an ultrasonicelectrochemical reactor. They investigated the effects of factors such as current density, ultrasonic power, and solution pH on the degradation process using mathematical methods. The results showed that at a pH of 2.7, a 95 % degradation efficiency was achieved after 2 h of degradation [37]. assess the mineralization efficiency ultrasound-electrochemical catalytic system, total organic carbon (TOC) analysis was performed. As depicted in Fig. 2f, the TOC removal efficiency was enhanced by 3-fold at 2 h (from 12.1 % to 36.3 %) when 280 W ultrasound was introduced into the system under a 15 mA applied current (Table 1). The synergistic improvement in degradation efficiency and TOC removal might be attributed to the ultrasonic cavitation effect, which promotes the generation of reactive species such as H₂O₂ and facilitates mass transfer at the electrode interface.

The results demonstrate that the degradation efficiency of OFL exhibits a notable upward trend with the increase in ultrasonic power. As shown in Fig. 2e, the degradation efficiency with power of 360 W is 2.47 times higher than that at 200 W after 15 min degradation, increasing from 24.9 % to 61.5 %. However, when the ultrasonic power was increased from 280 W to 360 W, although the reaction rate was faster in the first 15 min, the degradation efficiency at 30 min plateaued at a level comparable to that at 280 W. This indicates that the overall degradation rate did not increase linearly with the higher power. Therefore, considering the energy consumption and the principle of diminishing returns, 280 W was selected as the standard ultrasonic power for subsequent experiments. With the increase of ultrasonic power, the mass transfer in the system was enhanced by the microjets and crush of microbubbles, and more ROS were produced to degrade organic contaminants [38]. This largely overcomes the mass transfer limitations in conventional electro-Fenton reactions that may arise from the ion layer density on the electrode surface and the lack of stirring in

the solution, thereby helping to increase the reaction rate. When high-frequency ultrasound is applied, microbubbles in the solution rapidly expand and collapse violently after reaching a critical size, generating localized high temperatures and pressures that promote the formation of free radicals [39]. Furthermore, ultrasound can be regarded as a form of mechanical vibration, and the shear forces generated by it can promote the cleavage of organic molecular structures to a certain extent. Increasing ultrasonic power facilitates mass transfer and the generation of reactive species like H2O2 and hydroxyl radicals. However, excessively high power may incur unnecessary energy consumption, thus impeding large-scale implementation. To clarify the energy consumption of the system after the introduction of ultrasound, the corresponding calculations were performed. In our study, the ultrasonic power was set to 280 W, the applied current to 15 mA, and the corresponding voltage to 1.2 V. Each experiment was conducted for 30 min, so the total energy consumption of each experiment was calculated to be approximately:

 $\begin{aligned} &E_{total} = Power \times Time = (1.2V \times 0.015A + 280W) \times 0.5h/1000 \\ &= 0.140009 \text{ kWh} \end{aligned}$

Each experiment involved 150 mL of 25 mg/L OFL solution, corresponding to a total pollutant mass of:

 $0.15 L \times 25 mg/L = 3.75 mg$ (0.00375g) of OFL

Therefore, the degradation efficiency per kWh was calculated as:

0.00375g / 0.140009 kWh = 0.02678g/kWh = 26.78mg/kWh

In comparison, other similar ultrasound-assisted electro-Fenton systems typically degrade approximately 29.89 mg of OFL per kilowatthour of energy consumed [37]. This represents a relatively outstanding performance for our Fe-MG system, demonstrating the system's efficient utilization of energy.

 $0.15L\times50mg/L\times0.9~/0.140009~kWh=48.21mg/kWh$

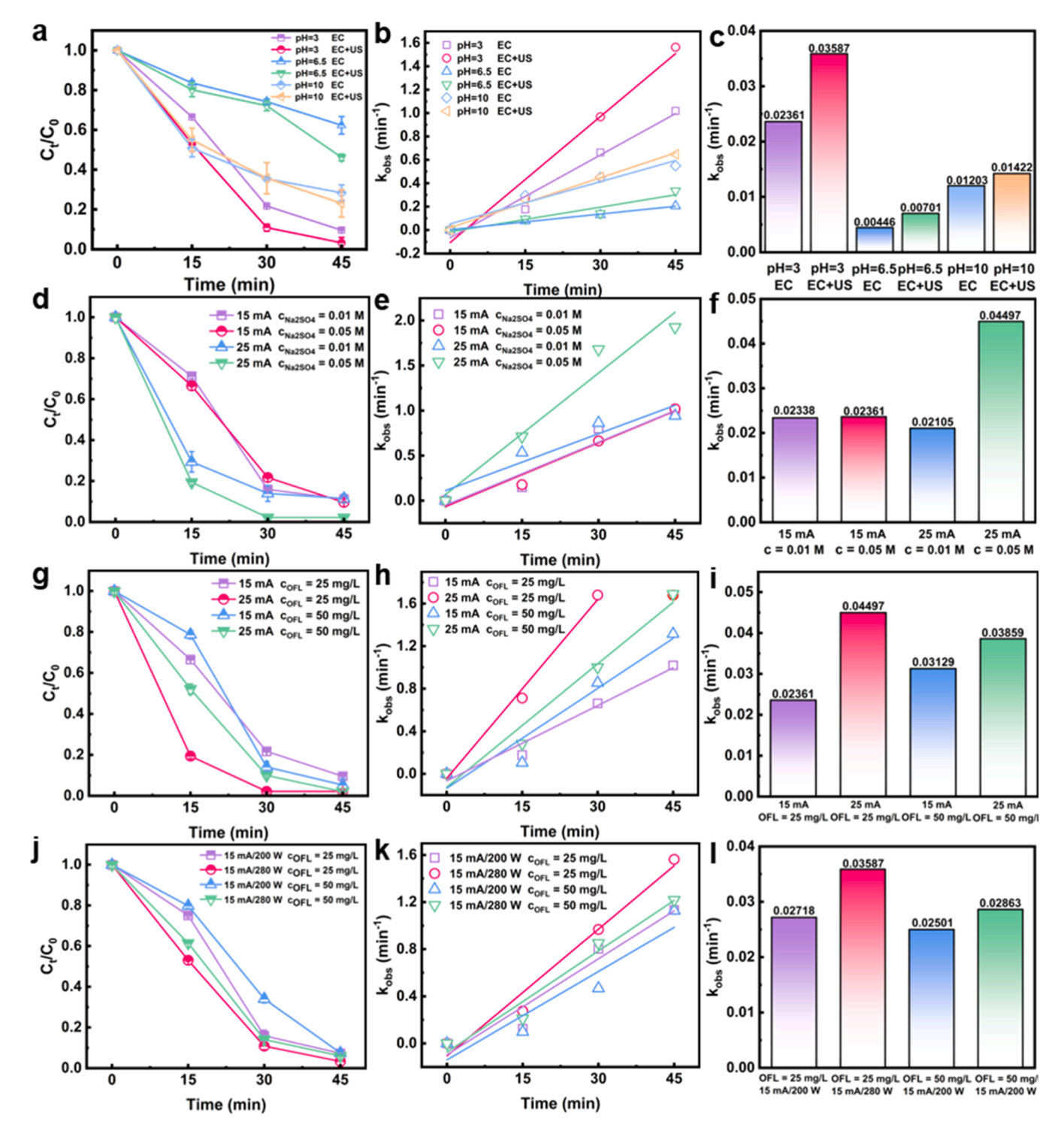


Fig. 3. (a-c) Degradation efficiency, and kinetics of OFL under different pH values, (d-f) degradation efficiency, and kinetics of OFL under different Na_2SO_4 concentrations, (g-l) effects of OFL concentrations on degradation efficiency, and kinetics with and without ultrasonic loading.

Table 1Comparison of TOC mineralization efficiencies under different conditions.

Current intensity (mA)	Ultrasonic power (W)	Time (h)	TOC removal (%)
15	/	1	12.10
15	280	1	15.42
15	/	2	12.10
15	280	2	36.30

The assessment of an AOP's optimal performance must integrate energy cost alongside degradation efficiency. Our system achieves high degradation with an energy consumption of 48.21 mg/kWh, a rate that is competitive with analogous systems. This favorable energy footprint exemplifies the practical energy trade-off considered in our work.

3.2. The effect of operational parameters on the US/EC degradation process

3.2.1. The effect of pH

In the electro-Fenton system, the solution pH is a pivotal parameter. Variations in acidity not only govern the speciation of iron ions but also regulate radical generation via competing side reactions [40]. The initial solution pH values were set as 3 (acidic), 6.5 (near-neutral) and 10 (alkaline) to explore the effect of initial pH on the degradation of OFL. As depicted in Fig. 3a, the electrochemical system using Fe-MG exhibits the highest degradation capacity in acidic solutions. Under a 15 mA applied current, the degradation efficiencies at 45 min were 90.4 % (pH = 3), 37.7 % (pH = 6.5), and 71.7 % (pH = 10). As evidenced in Fig. 3c, this trend was accentuated with the application of ultrasound. With 280 W ultrasound, the reaction constants in acidic solution (0.03587 min⁻¹) were 5.12-fold and 2.52-fold those in neutral solution $(0.00701 \text{ min}^{-1})$ and alkaline solution $(0.01422 \text{ min}^{-1})$, respectively. Among them, the degradation reaction exhibited the lowest rate under neutral conditions. Under a 15 mA applied current, only 35.2 % of OFL was degraded at 45 min. Even after the introduction of ultrasound, the degradation efficiency was only 45.1 % within 45 min. Concurrently, notable brown precipitates formed in the solution during the reaction under both neutral and alkaline conditions. This phenomenon is likely associated with the speciation of iron ions and the generation dynamics of free radicals. In acidic solutions (particularly at pH = 3), iron ions maintain high solubility, enabling continuous participation in the reaction [41]. The Fe^{2+}/Fe^{3+} redox couple further activates H_2O_2 to generate free radicals [42,43]. However, when the pH exceeds 4, ferric ions tend to precipitate as Fe(OH)3, causing a gradual decrease in the concentration of soluble iron species and a subsequent reduction in reaction efficacy. Notably, hydrogen peroxide (H2O2), a crucial reactant in the Fenton reaction, predominantly exists in its molecular form under acidic conditions, which facilitates its reaction with ferrous/ferric ions to generate •OH. Conversely, excessively low pH values may promote competitive reactions between H⁺ and •OH [44], thereby impeding the primary degradation process. Moreover, an excessively low pH value in the solution will exacerbate corrosion, posing substantial challenges to the maintenance of reaction equipment and the practical application of the degradation process. The choice of pH 3 was driven by the well-established prerequisites for an efficient Fenton process, which was further validated by experimental data of this study and is in strong agreement with extensive prior research.

3.2.2. The effect of electrolyte concentration

The concentration of electrolyte serves as a critical parameter in electrochemical reactions. To investigate the impact of electrolyte concentration on the degradation, degradation experiments with different electrolyte concentrations were conducted. The electrolyte concentrations were set at 0.01 M and 0.05 M, respectively. As depicted in Fig. 3d, the OFL removal efficiency exhibited a marked increase with the Na₂SO₄ concentration escalating from 0.01 M to 0.05 M. Under a 25 mA applied current, the removal efficiencies were 97.8 % (0.05 M) and 86.0 % (0.01 M), respectively. The corresponding reaction constants also showed a 2.14-fold increase (from $0.02105~\text{min}^{-1}$ to $0.04497~\text{min}^{-1}$). Meanwhile, there is a notable increase in the internal resistance of the reaction system. The electrolyte concentration is inherently linked to electron migration rate and solution conductivity. Extremely low electrolyte concentrations enhance solution internal resistance, thereby restricting electron transfer rate [45]. However, excessive concentration of electrolyte may lead to the formation of a thin film composed of inorganic salts on the electrode surface, thereby hindering the contact between organic contaminants and electrodes [46]. To further investigate the degradation capability of the Fe-MG system for OFL in solutions with compositions closer to actual water bodies, degradation experiments were conducted with the addition of extra inorganic ions and natural organic matter. Chloride ions (Cl-) and bicarbonate ions are

inorganic ions commonly found in wastewater [47]. Humic acid, as a common type of natural organic matter (NOM) in advanced oxidation process research, was also added to the experiments [48]. The presence of these matters may affect the reaction process by influencing the reaction kinetics or participating in competitive reactions. As shown in Fig. S2, despite observable inhibition by NOM and inorganic ions in the early stage, the overall reaction constant in the complex water matrix (0.16200 $\rm min^{-1}$) was ultimately very similar to that in pure water (0.15267 $\rm min^{-1}$) after 20 min reaction. This demonstrates that the negative impact of the complex background was negligible over the complete treatment cycle.

3.2.3. The effect of OFL concentration

The initial antibiotic concentration also has a significant impact on the reaction, notably influencing the degradation kinetics during the early phase. To investigate the concentration-dependent degradation characteristics in the degradation process, initial concentrations of OFL were set as 5 mg/L, 25 mg/L and 50 mg/L. The concentration of 5 mg/L was chosen primarily to investigate the degradation performance of the Fe-MG system under conditions where the OFL concentration is closer to that in real environments (typically in the range of $\mu g/L$ to mg/L [49]). As shown in Fig. 3 g, increasing the initial OFL concentration from 25 mg/L to 50 mg/L led to a notable decrease in the initial degradation rate. At 15 min under a 25 mA applied current, the degradation efficiencies were 80.6 % (25 mg/L) and 47.9 % (50 mg/L), respectively. The corresponding reaction constants also dropped from 0.04497 min⁻¹ to 0.03859 min⁻¹. This phenomenon can be attributed to competitive adsorption, wherein an excess of antibiotic molecules and intermediate products occupy the active sites on the catalyst surface at different reaction stages, thereby hindering mass transfer and inhibiting overall reaction kinetics. Additionally, when pollutant concentration increases, if the generation rate of reactive oxygen species (ROS) fails to match the rise in contaminant concentration, this mismatch will also result in a decrease in degradation efficiency [50]. When treating wastewater with low OFL concentration (5 mg/L), the Fe-MG system still maintains high degradation capability, achieving complete degradation of OFL in only 15 min at a current of 25 mA, as shown in Fig. S1a. The degradation rate does not show a significant decrease due to the reduction of reactants in the solution, demonstrating the adaptability of the Fe-MG system to different environments. It is worth noting that the relationship between the degradation rate and the change in pollutant concentration is not a simple linear one. Many factors in the reaction may affect the progress of the main reaction, such as the formation of intermediate products and the accompanying competitive reactions for free radicals. The intermediates generated in reaction process can also be an obstacle for the degradation of the original target contaminants.

3.3. Morphology characterization of electrode

The surface morphology changes of Fe-MG before/after reactions were observed by SEM in Fig. 4. Fig. 4a reveals that the pristine Fe-MG ribbon features a relatively smooth surface morphology, free of discernible pits or protrusions. Following 30 min of electrochemical degradation under a 15 mA applied current (Fig. 4b), cluster structures with diameters ranging from 5 to 10 micrometers emerged on the ribbon surface, accompanied by attached sheet-like structures. At a higher applied current (25 mA), the compactness of the cluster structures was further enhanced. Notably, the application of ultrasonic irradiation rendered the distribution of these clusters more uniform across the ribbon surface. This phenomenon can be attributed to intensified oxidative reactions at elevated current intensities, which induce localized corrosion and exfoliation of surface layers, thereby exposing additional active sites for sustained catalytic activity. Ultrasound accelerates mass transfer in the system, homogenizes substance distribution, and exposes more active sites [51]. This explains why the cluster structures on the ribbon surface become more uniform with ultrasonic irradiation.

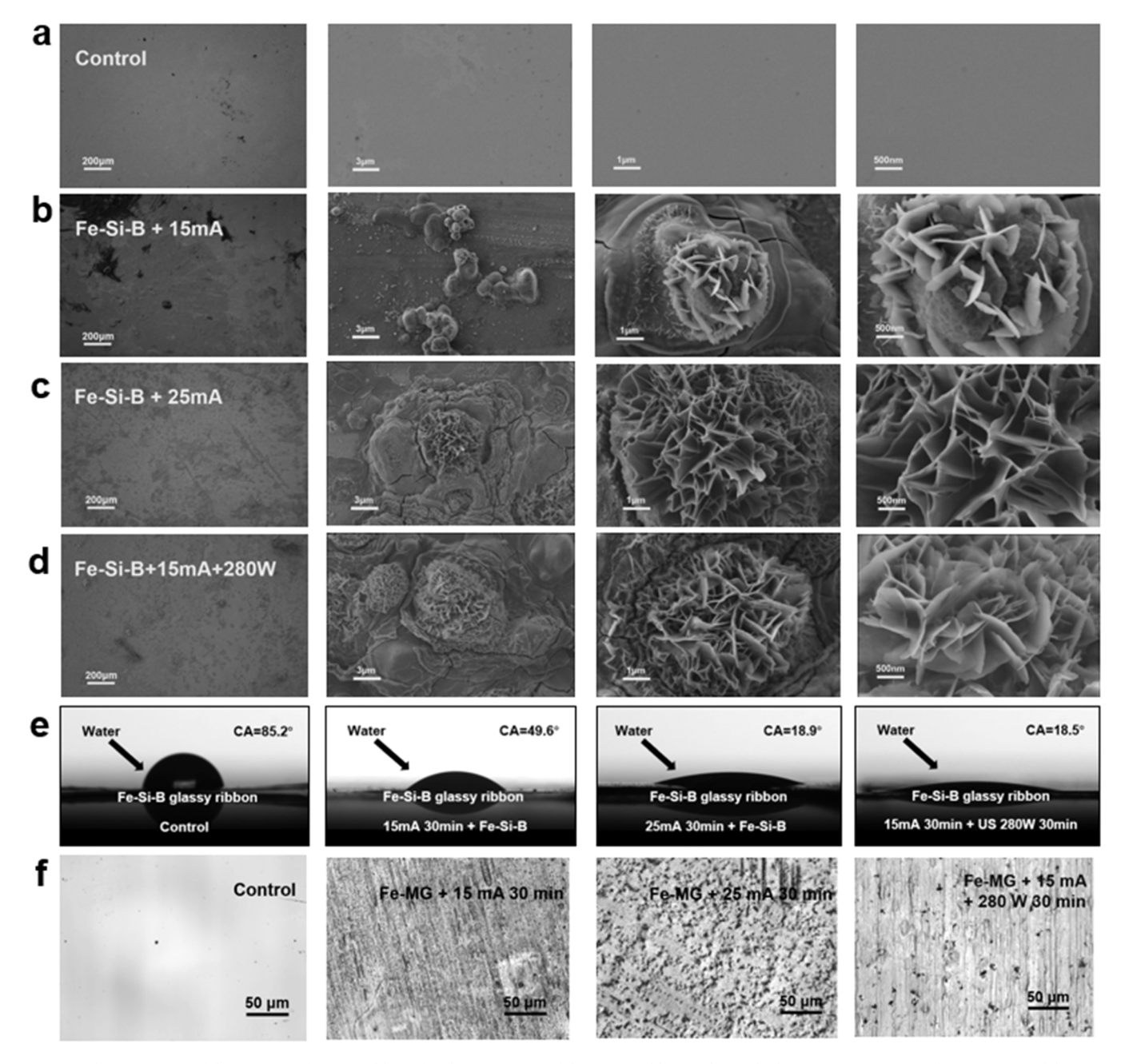


Fig. 4. (a) The SEM image of the as-received Fe-MG ribbon, (b) The SEM image of the Fe-MG ribbon under applied current (15 mA), (c) The SEM image of the Fe-MG ribbon under applied current (25 mA), (d) The SEM image of the Fe-MG ribbon under applied current (15 mA) and ultrasound loading (280 W), (e) The water contact images of the as-received Fe-MG ribbon, Fe-MG ribbon under applied current (15 mA) for 30 min, Fe-MG ribbon under applied current (25 mA) for 30 min, Fe-MG ribbon under applied current (15 mA) and ultrasound loading (280 W) for 30 min, Fe-MG ribbon under applied current (15 mA) for 30 min, Fe-MG ribbon under applied current (15 mA) and ultrasound loading (280 W) for 30 min, Fe-MG ribbon under applied current (15 mA) and ultrasound loading (280 W) for 30 min, Fe-MG ribbon under applied current (15 mA) and ultrasound loading (280 W) for 30 min.

Meanwhile, it is noteworthy that the formation of surface cluster structures via increased current intensity and ultrasonic introduction is accompanied by a substantial change in the hydrophilicity of the electrode surface. The hydrophilicity of the electrode surface was measured by water contact angle testing. As shown in Fig. 4e, the water contact angle of the pristine Fe-MG was 85.2° , while the contact angles after electrochemical reactions were 49.6° (15 mA) and 18.9° (25 mA). Simultaneously, the uniform distribution of cluster structures induced by ultrasound was accompanied by a notable decrease in the contact angle of the material, which decreased to 18.5° . To quantitatively analyze the relationship between changes in the material's surface structure and hydrophilicity, a confocal laser scanning microscopy

(CLSM) test was conducted. The specific data regarding the changes in surface roughness of the ribbons before and after the reaction are listed in Table 2. Combined with the previous SEM results, the application of

 $\begin{tabular}{ll} \textbf{Table 2} \\ \textbf{Surface roughness parameters of the Fe-MG ribbons under different reaction conditions.} \end{tabular}$

Current intensity (mA)	Ultrasonic power (W)	Surface Roughness (μm)	
/	/	0.202	
15	/	1.245	
25	/	1.740	
15	280	1.023	

current promotes the formation of cluster structures on the ribbon surface, which is also accompanied by an increase in the ribbon's surface roughness. After operating at currents of 15 mA and 25 mA for 30 min respectively, the surface roughness of the ribbon increases to $1.245 \mu m$ and 1.740 µm. While the surface roughness of the pristine ribbon is $0.202~\mu m$. These quantitative roughness data (1.2–2.0 μm) align with the observed enhancement in hydrophilicity. The increased roughness amplifies the effective surface area and capillary effects, which directly promotes liquid spreading, this is consistent with the Wenzel wetting model [52]. As the surface roughness increases, the contact angle of the hydrophilic material surface gradually decreases [53]. All these results indicate that increasing the current intensity and introducing ultrasound during the degradation process facilitate the formation of cluster structures with varying scales on the electrode surface. This increases the specific surface area of the electrode, exposes more active sites, and enhances the contact between pollutants and the electrode. Correspondingly, the generation of these surface structures also induces changes in the contact angle of the ribbons, leading to improved hydrophilicity that promotes catalytic reactions at the solid-liquid interface.

3.4. EDS analysis

EDS analysis was conducted to investigate the elemental changes on the ribbon surface before and after the reaction. As illustrated in Fig. 5, the elemental distribution on the ribbon surface after the reaction differs markedly across various reaction conditions. The changes in the content of each element before and after the reaction are listed in Table 3. The Fe-to-Si content ratio in pristine Fe-MG ribbons was 89.5:9.7, which aligns with the original proportion of $Fe_{78}Si_9B_{13}$, accounting for the

Table 3Summary of the elemental composition variation for the Fe-MG ribbon under various reaction conditions

Current intensity (mA)	Ultrasonic power (W)	Fe (%)	Si (%)	O (%)
/	/	89.16	9.51	1.33
15	/	24.85	1.27	62.93
25	/	23.42	1.41	62.41
15	280	21.36	1.67	61.59

absence of B in the energy spectrum. Following electrochemical degradation at 15 mA for 45 min, the central Fe and Si concentrations in cluster structures declined substantially, while the O concentration rose markedly. The Fe content dropped to 24.9 %, the Si content fell below 2 %, and the oxygen content rose to 62.9 %. In the relatively flat regions away from the cluster structures, the Fe and Si contents were higher than those in the central areas, and the Fe-to-Si ratio remained close to the pre-reaction level (49:4.5). These results suggest that an oxidation reaction of a certain degree occurred in the vicinity of the cluster structures on the ribbon surface, with Fe and Si leaching into the solution [54]. As the current increases, this trend becomes even more pronounced, with Fe, Si, and O contents reaching 23.42 %, 1.41 %, and 62.41 %, respectively. Upon introducing ultrasound into the system, similar elemental changes were observed in the ribbons. The combined analysis of elemental content variations and SEM images indicates that a vigorous oxidation reaction has occurred on the ribbon surface [55]. The leaching of Fe and Si enables continuous exposure of more catalytic sites on the electrode surface. Such surface reconstruction generates catalytically active sites, which are essential for maintaining sustained degradation efficiency.

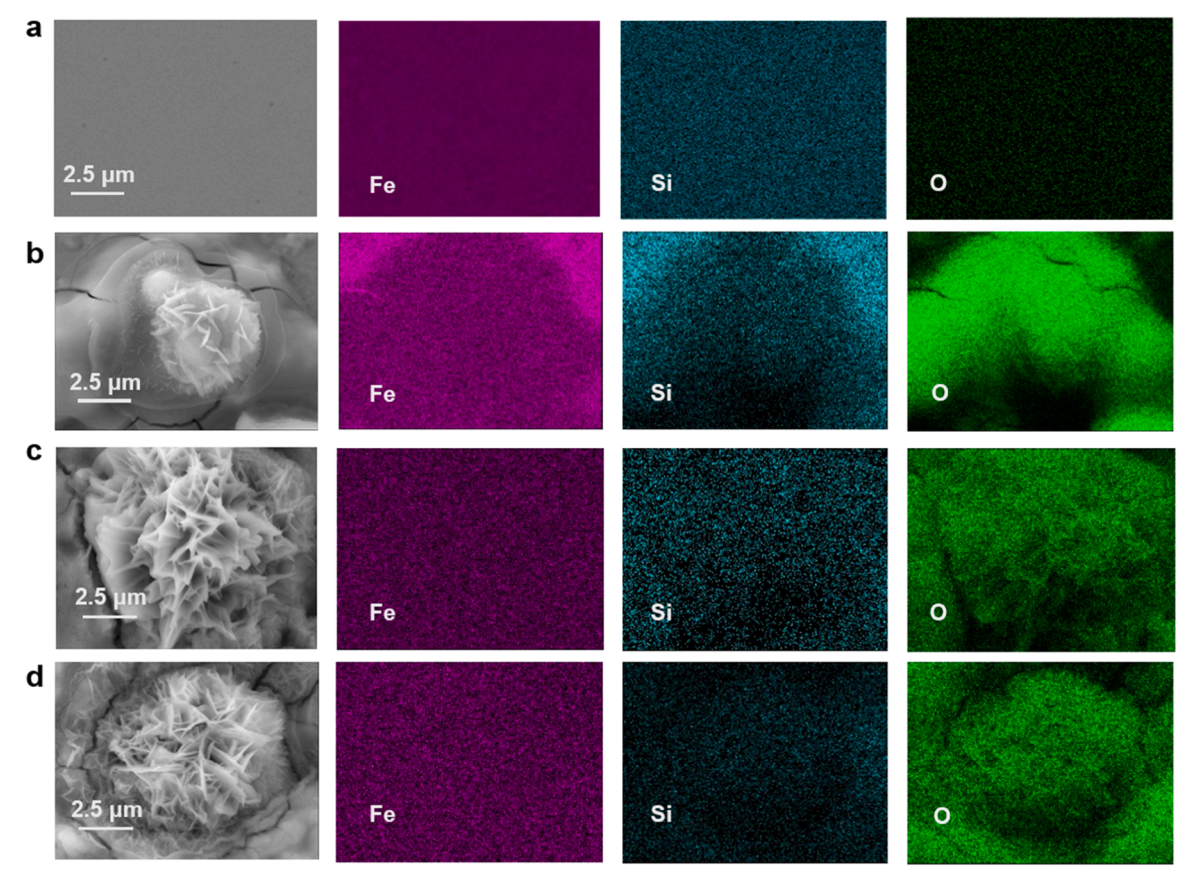


Fig. 5. (a) The SEM image and EDS spectra of the as-received Fe-MG ribbon, (b) The SEM image and EDS spectra of the Fe-MG ribbon under applied current (15 mA), (c) The SEM image and EDS spectra of the Fe-MG ribbon under applied current (25 mA), (d) The SEM image and EDS spectra of the Fe-MG ribbon under applied current (15 mA) and ultrasound loading (280 W).

3.5. XPS analysis

As shown in Fig. 6, X-ray photoelectron spectroscopy (XPS) was performed on Fe-MG ribbons under different reaction conditions to systematically explore elemental valence state variations during the reaction. The pristine Fe-MG ribbon displayed characteristic binding energies for Fe 0 (706.76 eV), Fe $^{2+}$ (710.68 eV), Fe $^{3+}$ (713.91 eV), B–B (191.85 eV), B–O (187.71 eV), Si–Si (101.94 eV), Si–O (99.07 eV), Fe–O (529.88 eV), and O-M (531.58 eV), serving as a baseline for monitoring valence state changes in subsequent reactions. In the pristine Fe-MG ribbons, the main iron valence states were Fe 0 , Fe $^{2+}$, and Fe $^{3+}$.

By comparing the areas of characteristic peaks, the valence state variations of substances can be determined in XPS spectra. As shown in Fig. 6b, after reacting for 45 min under 15 mA, the surface of Fe-MG ribbons exhibited only two valence states of Fe²⁺ and Fe³⁺ with the Fe⁰ content dropping to zero. The disappearance of the Fe⁰ characteristic peak suggests that upon oxidation, the Fe⁰ on the ribbon surface was converted into oxides that coat the ribbon surface [54]. Meanwhile, the total Fe 2p signal also showed a substantial decrease after the reaction, which was attributed to the formation of FeOOH as observed in Fig. 6b.

The generated FeOOH facilitates the reduction of Fe³⁺ to Fe²⁺ through interactions with reductive species in the solution, which may be the main regeneration pathway of Fe(II) of the system, thereby maintaining catalytic activity and enhancing degradation efficiency. Additionally, FeOOH exhibits intrinsic catalytic ability to decompose hydrogen peroxide, promoting hydroxyl radical generation. Fig. 6d illustrates remarkable valence state changes after the reaction with ultrasonic irradiation. Complete depletion of Fe⁰ species was observed, accompanied by an increase in Fe²⁺ content from 63.8 % to 67.9 %. Concurrently, the total Fe 2p signal intensity decreased by 37.5 %, indicating substantial Fe leaching into the solution and subsequent participation in redox processes via higher valence states. These findings confirm that the oxidative conversion of Fe⁰ to Fe²⁺/Fe³⁺ dominates the redox cycle during organic pollutant degradation, with continuous cycling between these oxidized states. Additionally, it is noteworthy that compared with electrochemical degradation alone, the contents of B-B and Si-Si bonds increased after ultrasound-assisted electrochemical degradation. Elevation of the current intensity induced progressive depletion of silicon-containing bonds, as evidenced by the total Si 2p signal intensities in Fig. 6b and Fig. 6c, which declined by 42.9 % and 43.8 %,

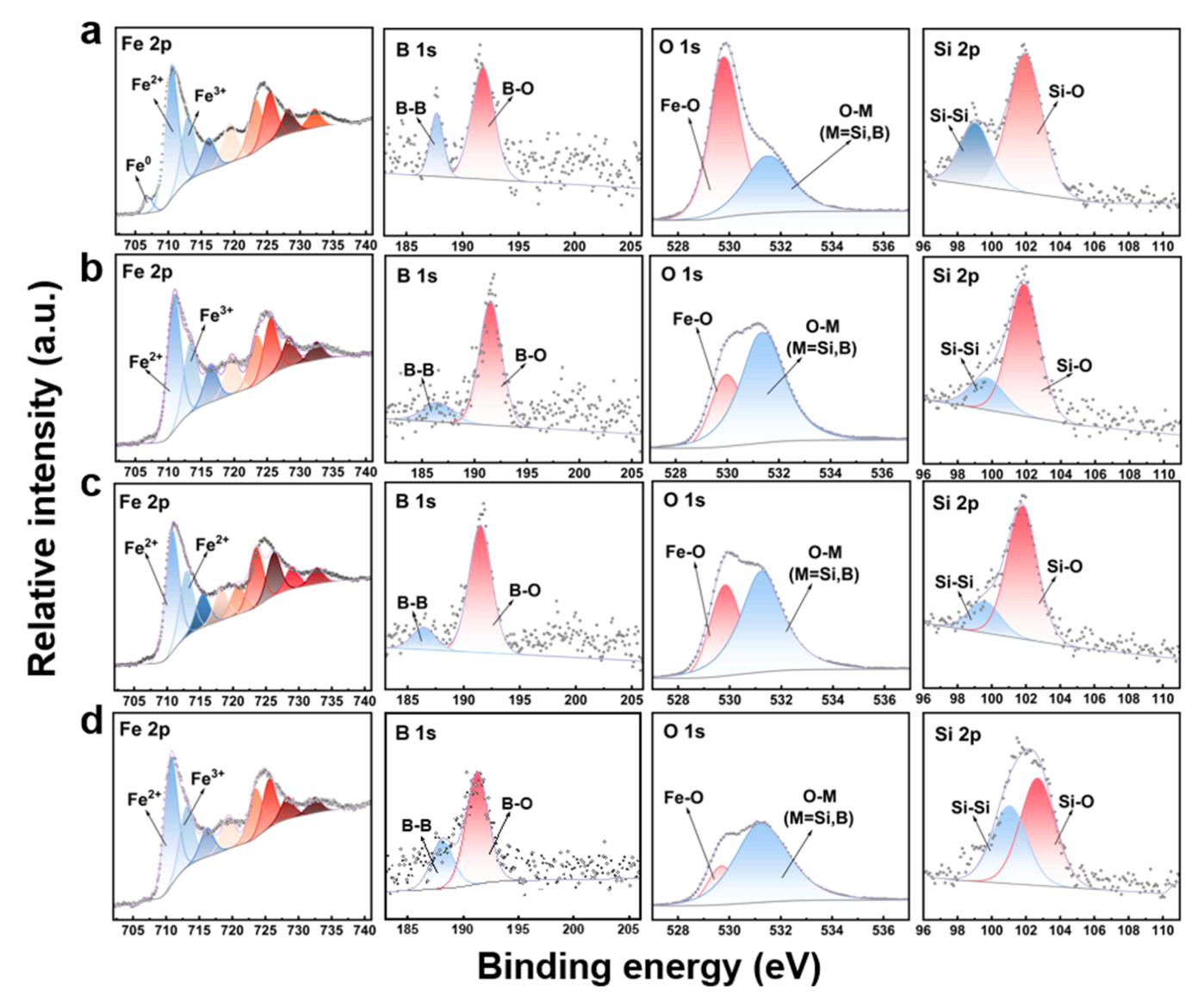


Fig. 6. The XPS spectra of (a) Fe 2p, B 1 s, O 1 s and Si 2p for the as-received Fe-MG ribbon, (b) Fe 2p, B1 s, O 1 s and Si 2p for the Fe-MG ribbon under applied current (15 mA), (c) Fe 2p, B 1 s, O 1 s and Si 2p for the Fe-MG ribbon under applied current (15 mA), (d) Fe 2p, B 1 s, O 1 s and Si 2p for the Fe-MG ribbon under applied current (15 mA) and ultrasound loading (280 W).

respectively. This suggests the synergistic leaching of Si and Fe species, which may facilitate the formation of micro-nano surface structures on Fe-MG ribbons during the reaction. In Fig. 6, the O1s orbital indicates that oxygen exists in the form of metal oxides (Fe-O) and metal-like oxides (O-B, O-Si). The decrease in the content of metal oxides and the increase in the content of metal-like oxides before and after the reaction also suggest that during the degradation process, the metal-like elements on the electrode surface are oxidized and participate in the redox reaction together with Fe [56].

3.6. Reaction mechanism

Electron paramagnetic resonance (EPR) tests were performed to identify the main types of reactive oxygen species (ROS) in the degradation process. The characteristic signal peaks of DMPO-•OH were captured by using DMPO as a trapping agent. The signal exhibited characteristic peak intensity ratios of 1:2:2:1, which was identified as hydroxyl radicals (•OH) [57]. Notably, as shown in Fig. 7c, a signal with

characteristic peak intensity ratios of 1:1:2:2:4:2:2:1:1 was also captured by DMPO, which was identified as hydrogen radicals (\bullet H). To further confirm the generation of \bullet H, TEMPO was used as a probe. When TEMPO combines with \bullet H, its characteristic peak intensity decreases due to TEMPO consumption. As shown in Fig. 7a, the TEMPO intensity slightly declined with reaction progression, indicating the generation of a certain amount of \bullet H. Conversely, as depicted in Fig. 7b, the characteristic peak intensity of singlet oxygen ($^{1}O_{2}$) exhibited no marked variation throughout the reaction, indicating that $^{1}O_{2}$ was not substantially generated and thus was not the primary ROS in the system.

To further confirm the actual contribution of free radicals to the reaction, quenching experiments were conducted. TBA and PMSO were used as scavengers to quench •OH and high-valent iron species (Fe(IV)), respectively. As shown in Fig. S3, after the addition of 100 mM TBA and 2 mM PMSO, the degradation efficiency dropped to 80.72 % and 99.6 % of the previous value, respectively, indicating that •OH are the primary active species contributing to the reaction, while high-valent iron species do not make a significant contribution to OFL degradation. This is

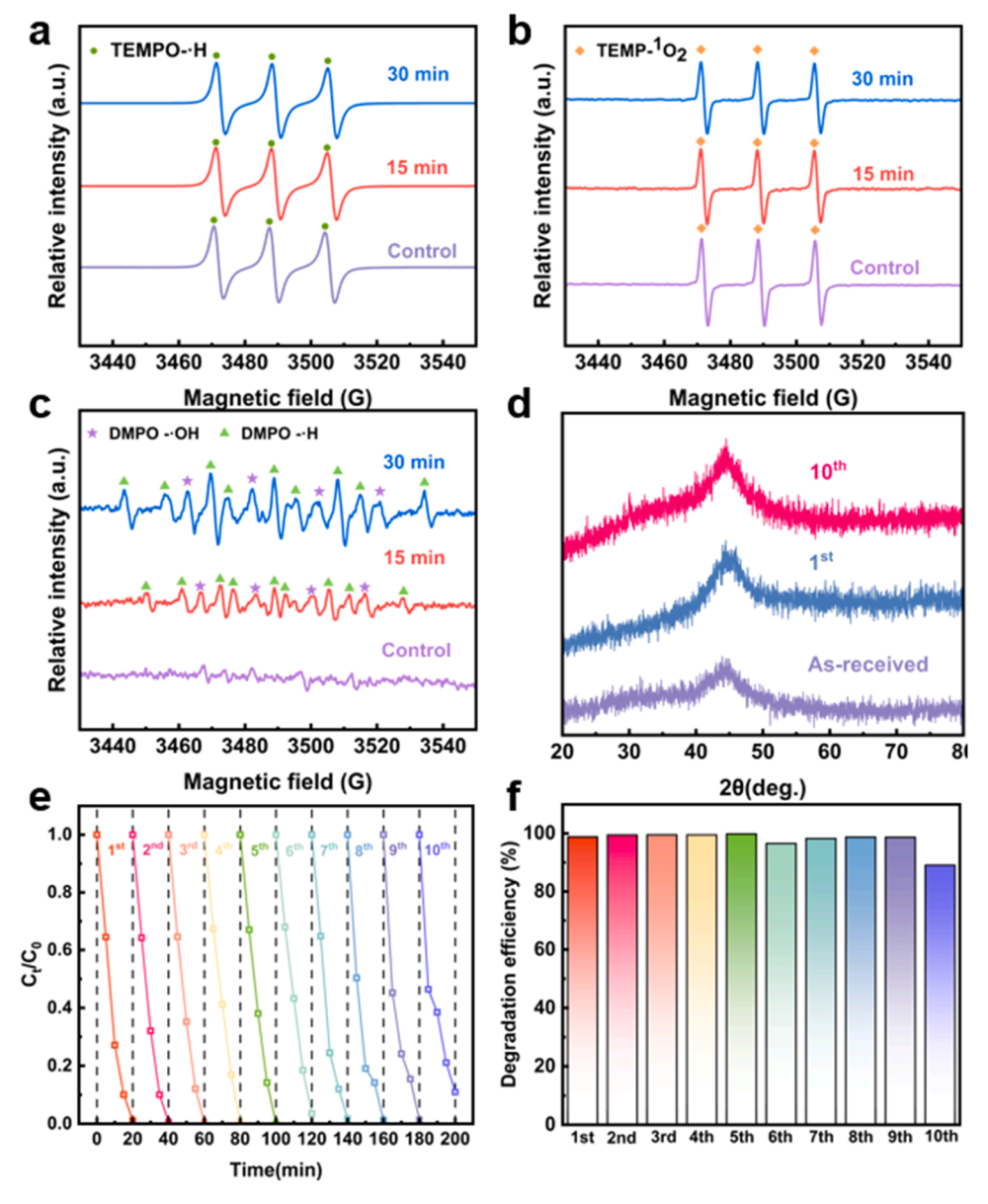


Fig. 7. (a-c) EPR spectra of TEMPO-♦H, TEMP-¹O₂, DMPO-♦OH+♦H generated by EC-US activated Fe-MG ribbon, (d) XRD image of the as-received Fe-MG ribbon, Fe-MG ribbon after one and ten reuse cycles, (e-f) degradation efficiency of Fe-MG ribbon in ten reuse cycles under applied current (15 mA) and ultrasound loading (280 W).

consistent with the previous experimental results in EPR tests. Due to the low yield and extremely short lifetime of •H, as well as the lack of specific quenchers, it is difficult to specifically detect them in quenching experiments. However, we believe that the enhanced intensity of the characteristic signal peak of its adduct after the addition of TEMPO provides strong evidence for the generation of hydrogen radicals. All these results confirmed that the ultrasound-assisted electrochemical degradation for OFL is a radical process, •OH and •H are main ROS in degradation process. Hydroxyl radicals, recognized for their strong oxidizing properties, play a pivotal role in advanced oxidation processes (AOPs), where they degrade organic contaminants into smaller molecular fragments or less toxic compounds through oxidative attack. Compared with strong oxidizing radicals such as hydroxyl radicals, hydrogen radicals, as a reducing radical, exhibit a notable promoting effect on the electrocatalytic reduction of N₂ [58], though they have not been extensively investigated in wastewater treatment. In the Fe-MG system, the primary pathway for the generation of hydrogen radicals is likely the initial step of the cathodic hydrogen evolution reaction, as indicated by Eq. (4). The generation of hydrogen radicals can promote the occurrence of oxygen reduction reactions (ORR) to produce H₂O₂. As an important reactant in Fenton-like systems, the yield of H₂O₂ is closely associated with the degradation efficiency of the system. This facilitates the progression of the electro-Fenton reaction [59]. It is hypothesized that hydrogen radicals (•H) originate from hydrogen ions (H⁺) in the aqueous medium. Concurrently, the homolytic cleavage of C-H bonds in OFL might also give rise to •H. These hydrogen radicals react with dissolved oxygen in the solution to form peroxyl radicals (HOO•), which subsequently combine with another •H to yield H₂O₂.

$$H_3O^+ + e^- \rightarrow H + H_2O$$
 (4)

$$H + O_2 \rightarrow OOH$$
 (5)

$$OOH + H \rightarrow H_2O_2 \tag{6}$$

Meanwhile, these two radical species synergistically drive opposing redox reactions, collectively enhancing pollutant degradation efficiency. As the reaction proceeds, uneven charge distribution induces localized enrichment of H⁺ at specific regions of the electrode surface. This spatial accumulation creates a strong electric field between H⁺ and hydroxyl ions (OH) [60]. In this scenario, •OH loses electrons to form hydroxyl radicals (•OH), while H⁺ gains electrons to generate •H.

Understanding the reactions occurring on the electrode surface during the degradation process is conducive to gaining in-depth insights into the reaction mechanism. To this end, the potential reactions near the cathode and anode in the Fe-MG system were analyzed. The reactions that may occur at the anode are as follows:

$$Fe \rightarrow Fe^{2+} + 2e^{-} \tag{7}$$

$$2H_2O \rightarrow O_2 + 4H^+ + 4e^-$$
 (8)

$$OFL \rightarrow Oxidation \ products + ne^-$$
 (9)

$$Fe^{2+} \to Fe^{3+} + e^{-}$$
 (10)

The main reaction at the anode is the dissolution of Fe, where Fe on the electrode surface is oxidized into ionic form and enters the solution to participate in subsequent reactions, serving as the primary source of ${\rm Fe}^{2+}$ for the Fenton reaction [61], as shown in Eq. (7). At the same time, several competitive side reactions that can reduce current utilization efficiency may occur near the anode, such as the oxygen evolution reaction (OER), the direct oxidation of OFL, and even the oxidation of ${\rm Fe}^{2+}$ entering the solution to form ${\rm Fe}^{3+}$. On the cathode side, the main reaction is the in-situ generation of ${\rm H}_2{\rm O}_2$, which is also the core reaction of the Fenton system [61], as shown in Eq. (11). It is worth noting that in the Fe-MG system, since we use an active electrode material as the cathode, it also provides a potential pathway for the reduction of Fe(II)

at the cathode, as shown in Eq. (15), Fe³⁺ in the solution receives electrons and is reduced to Fe²⁺, which facilitates the recycling of Fe in the solution. This reaction, together with the direct reduction of Fe(II) provided in Eq. (14), constitutes the main pathways for Fe(II) reduction in the system. The potential reactions at the cathode and in the solution are listed as follows:

$$O_2 + 2H^+ + 2e^- \rightarrow H_2O_2$$
 (11)

$$O_2 + 4H^+ + 4e^- \rightarrow H_2O$$
 (12)

$$2H^+ + 2e^- \rightarrow H_2(g)$$
 (13)

$$Fe^{3+} + e^{-} \rightarrow Fe^{2+}$$
 (14)

$$2Fe^{3+} + Fe \to 3Fe^{2+} \tag{15}$$

$$Fe^{2+} + H_2O_2 \rightarrow Fe^{3+} + OH + OH^-$$
 (16)

$$Fe^{3+} + H_2O_2 \rightarrow Fe^{2+} \rightarrow HO_2 + H^+$$
 (17)

Liquid chromatography-mass spectrometry (LC-MS) was used to detect the intermediate products of OFL degradation, and the possible degradation pathways were inferred. Four major intermediate products were detected by LC-MS and are listed in Table S4. As shown in Fig. 8, during the degradation of OFL, there are two possible degradation pathways. In pathway I, under the combined action of applied current and ultrasound, OFL is first decarboxylated, leading to the formation of TP1 (m/z = 318) through the loss of CO₂ (-44 Da). Subsequently, under further oxidation, reactions such as the ring-opening of the piperazine ring occur [62], leading to the gradual formation of TP3 (m/z = 223), TP4 (m/z = 205), and TP5 (m/z = 164), which are ultimately oxidized to CO₂, H₂O, or other small-molecule substances. The main difference in pathway II lies in the formation of initial products. Unlike pathway I, where decarboxylation occurs first, in pathway II, the piperazine ring of the OFL molecule is cleaved first to generate TP2 (m/z = 279) [63], followed by the gradual formation of subsequent products such as TP3, TP4, and TP5. These reactions illustrate that both decarboxylation and piperazine ring cleavage serve as primary degradation pathways. The final mineralization of OFL into CO2, H2O, and other small-molecule substances is consistent with the results of TOC tests.

3.7. Reusability of Fe-MG ribbons

To investigate the durability of Fe-MG ribbons during the electrochemical degradation of OFL, reusability degradation experiments were conducted. Additionally, X-ray diffraction (XRD) was performed on the ribbons before and after degradation to assess the stability of their microstructure. The results show that Fe-MG ribbon electrodes maintain remarkable stability during the degradation process. During reusability experiments, the electrode surfaces exhibit varying degrees of exfoliation. This phenomenon increases ribbon roughness, enhances the specific surface area, and continuously exposes fresh electrode material in deeper layers, collectively sustaining the catalytic reaction [64]. As depicted in Fig. 7d, XRD results reveal that Fe-MG ribbons exhibit typical broad scattering peaks at $2\theta = 40-50^{\circ}$ both before and after the reaction. This indicates that the electrode maintains a stable amorphous structure even after five reusability experiments [65]. As shown in Fig. 7e, f, the Fe-MG electrode can still maintain a degradation efficiency of over 90 % after 10 consecutive runs at a current of 15 mA and under 280 W ultrasound, demonstrating its superiority in stability and its potential for long-term, efficient, and stable operation as an electrode for large-scale wastewater degradation. Slight variations in degradation efficiency during cycling are likely due to surface oxide formation. Additionally, intermediate product generation may affect the adsorption performance of Fe-MG ribbons. The degradation performance of this study is compared with other similar AOP systems in Table 4. To

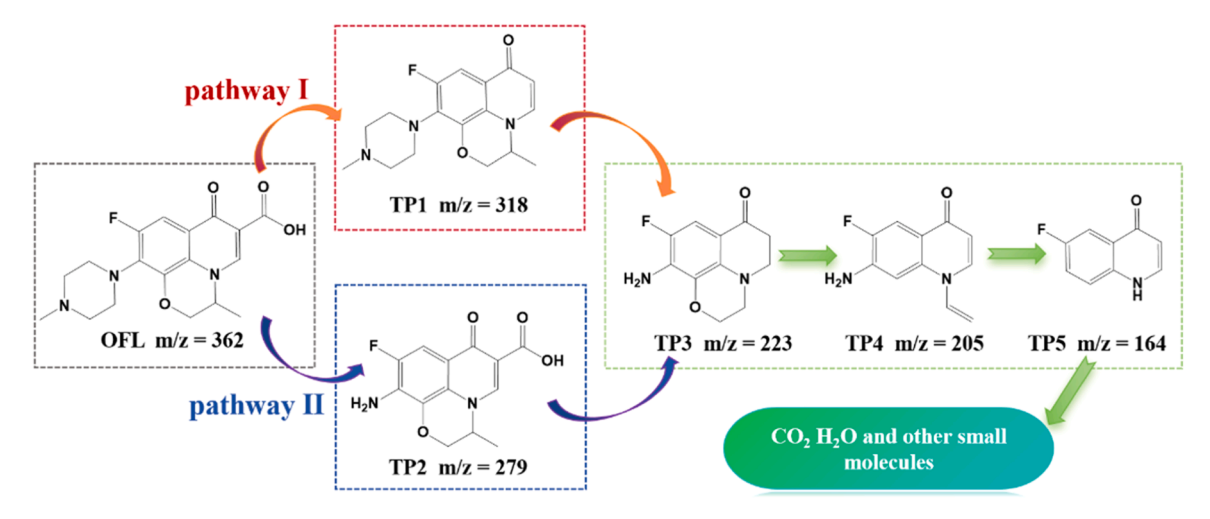


Fig. 8. Degradation pathway of OFL in Fe-MG system.

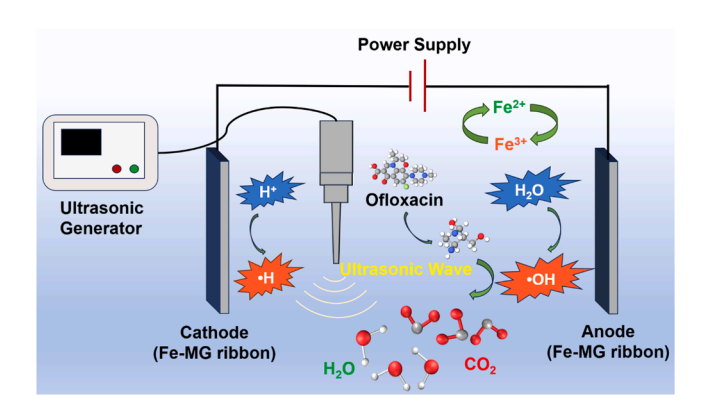


Fig. 9. Diagram of reaction mechanism of ofloxacin degradation in ultrasound-electrochemical system.

Table 4Comparative of the degradation performance of various AOPs for OFL removal.

Pollutant concentration	AOPs type	Materials	Experimental conditions	Degradation efficiency	Refs.
OFL; 25 mg/L	Sono/ electro- Fenton	Fe ₇₈ Si ₉ B ₁₃ metallic glass	[J] = 5 mA/ cm ² ; [P _{ultrasound}]= 280 W; t = 45 min	96.7 %	This work
OFL; 20 mg/L	Photo- Fenton	Y ₂ O ₃ / BiOCl	$\begin{aligned} &[P_{light}]\\ &= 300 \text{ W;}\\ &t = 120 \text{ min} \end{aligned}$	87.81 %	[29]
OFL; 25 mg/L	Electro- Fenton	Ti/carbon felt box	[Voltage] = 2 V; t = 105 min	100 %	[36]
OFL; 20 mg/L	Sono/ electro- Fenton	(Ti/ RuO ₂)/ stainless steel	$[J] = 213 \text{ A/}$ $m^{2};$ $[P_{ultrasound}]$ $= 56 \text{ W;}$ $t = 120 \text{ min}$	95 %	[37]

quantitatively determine the metal leaching during the degradation process, inductively coupled plasma-optical emission spectrometry (ICP-OES) was employed. The Fe content in the solution after the reaction was 22.69 mg/L. Correspondingly, for the degradation of an OFL solution with an initial concentration of 25 mg/L, this is equivalent to 0.9 mg of Fe being released into the solution in ionic form per milligram of OFL degraded. Since the concentration of antibiotics in actual wastewater is typically in the microgram to milligram range, we believe

that Fe leaching will be significantly reduced during the degradation of real wastewater. Meanwhile, the iron ions entering the solution in ionic form will transform between ${\rm Fe}^{2+}$ and ${\rm Fe}^{3+}$, further promoting the reaction. Therefore, we consider this level of leaching to be acceptable and not detrimental to the evaluation of the Fe-MG electrode's stability and degradation performance. The above results indicate that Fe-MG ribbons, as electrodes, can achieve multiple cycles of stable and efficient degradation of OFL, demonstrating good stability.

4. Conclusions

In summary, the ultrasound-assisted electrochemical degradation system based on Fe₇₈Si₉B₁₃ ribbons as electrodes emerges as a promising approach for water purification. Under optimal conditions (15 mA current, 45 min, pH=3), the system achieves 90.4 % removal efficiency for 25 mg/L OFL. The application of ultrasound markedly enhances both pollutant removal and mineralization efficiency. Increasing ultrasonic power from 0 to 280 W elevates the kinetic rate constant from 0.02361 min⁻¹ to 0.03587 min⁻¹, while the mineralization efficiency of OFL exhibits a 3-fold increase (from 12.1 % to 36.3 %). Anodic oxidation induces the formation of oxidized morphologies on the ribbon surface, with cluster-like structures (5-10 µm in diameter) emerging on the anode. Higher current intensities and the addition of ultrasound both enhance the formation of these morphologies, with ultrasound further promoting more uniform distribution of the oxidized structures. Meanwhile, the presence of these cluster-like structures alters the water contact angle of the ribbon surface, improving electrode hydrophilicity and further facilitating the reaction progression. EDS analysis reveals leaching of Fe and Si during the reaction, where surface exfoliation continuously exposes fresh active sites to sustain catalysis. Key influencing factors (pH, initial concentration, electrolyte concentration) were systematically evaluated, and ultrasound was found to reduce the water contact angle, enhancing material hydrophilicity. Hydroxyl radicals and hydrogen radicals were identified as the main reactive oxygen species. Notably, the degradation system demonstrates considerable stability and electrochemical catalytic performance. In terms of energy consumption, our system can degrade nearly 50 mg of pollutants per kilowatt-hour of energy consumed, which represents a significant advantage compared with similar ultrasound-assisted electro-Fenton systems and may be further improved as the pollutant concentration increases. In particular, compared with common advanced oxidation systems that require the addition of external oxidants, our system is more environmentally friendly and cleaner. It eliminates both the potential secondary pollution caused by oxidants and the costs associated with the storage and transportation of oxidant, thereby significantly

enhancing the environmental benignity of the system. This study reveals the system's remarkable enhancement in both degradation and mineralization efficiency, offering an innovative solution for antibiotic wastewater treatment.

CRediT authorship contribution statement

Xiong Liang: Writing – review & editing, Funding acquisition, Conceptualization. Changyong Liu: Conceptualization. Kunheng Zou: Investigation. Zhenxuan Zhang: Writing – review & editing, Supervision, Methodology, Funding acquisition, Formal analysis, Conceptualization. Wenqing Ruan: Methodology. Mengting Yang: Methodology. Yu Zhang: Writing – original draft, Methodology, Investigation, Formal analysis. Jiang Ma: Writing – review & editing, Conceptualization.

Declaration of Competing Interest

The authors declare that they have no known competing financial interests or personal relationships that could have appeared to influence the work reported in this paper

Appendix A. Supporting information

Supplementary data associated with this article can be found in the online version at doi:10.1016/j.jallcom.2025.184422.

References

- M.S. Javed, M.A. Nazir, Z. Shafiq, S. Ullah, T. Najam, R. Iqbal, M.A. Ismail, T. L. Tamang, S.S.A. Shah, Advanced materials for photocatalytic removal of antibiotics from wastewater, J. Alloy. Compd. 1010 (2025) 177926.
- [2] N. Li, J. Ye, H. Dai, P. Shao, L. Liang, L. Kong, B. Yan, G. Chen, X. Duan, A critical review on correlating active sites, oxidative species and degradation routes with persulfate-based antibiotics oxidation, Water Res. 235 (2023) 119926.
- [3] Q.Q. Zhang, G.G. Ying, C.G. Pan, Y.S. Liu, J.L. Zhao, Comprehensive evaluation of antibiotics emission and fate in the river basins of China: source analysis, multimedia modeling, and linkage to bacterial resistance, Environ. Sci. Technol. 49 (2015) 6772-6782.
- [4] K. Qin, Q. Zhao, H. Yu, X. Xia, J. Li, S. He, L. Wei, T. An, A review of bismuth-based photocatalysts for antibiotic degradation: insight into the photocatalytic degradation performance, pathways and relevant mechanisms, Environ. Res. 199 (2021) 111360.
- [5] X.C. Liu, Y.Y. Zhou, J.C. Zhang, L. Luo, Y. Yang, H.L. Huang, H. Peng, L. Tang, Y. Mu, Insight into electro-Fenton and photo-Fenton for the degradation of antibiotics: mechanism study and research gaps, Chem. Eng. J. 347 (2018) 379–397.
- [6] A. Ahmad, P. Kumar, S.P. Singh, Recent advancements in heterogeneous cathode catalysts for in-situ hydrogen peroxide synthesis in bio-electro-Fenton process and its application in wastewater treatment: a review, J. Environ. Chem. Eng. 13 (2025) 117109.
- [7] R. Chen, X. Liu, Y. Liang, K. Zhang, Y. Wang, C. Du, C. Zhang, Q. Li, S. Dong, J. Sun, M. Fan, Emerging strategies for cathode materials toward high-performance microbial fuel cells based on E-Fenton principle, Sep. Purif. Technol. 365 (2025) 132662
- [8] Y.-S. Ma, C.-F. Sung, J.-G. Lin, Degradation of carbofuran in aqueous solution by ultrasound and fenton processes: effect of system parameters and kinetic study, J. Hazard. Mater. 178 (2010) 320–325.
- [9] S. Anandan, V. Kumar Ponnusamy, M. Ashokkumar, A review on hybrid techniques for the degradation of organic pollutants in aqueous environment, Ultrason. Sonochem. 67 (2020) 105130.
- [10] K. Makino, M.M. Mossoba, P. Riesz, Chemical effects of ultrasound on aqueous solutions. Formation of hydroxyl radicals and hydrogen atoms, J. Phys. Chem. Lett. 87 (1983) 1369–1377.
- [11] F. Ghanbari, A. Hassani, S. Wacławek, Z. Wang, G. Matyszczak, K.-Y.A. Lin, M. Dolatabadi, Insights into paracetamol degradation in aqueous solutions by ultrasound-assisted heterogeneous electro-Fenton process: key operating parameters, mineralization and toxicity assessment, Sep. Purif. Technol. 266 (2021) 118533.
- [12] S. Wu, Y.H. Hu, A comprehensive review on catalysts for electrocatalytic and photoelectrocatalytic degradation of antibiotics, Chem. Eng. J. 409 (2021) 127739.
- [13] F. Yao, Y. Zhong, Q. Yang, D. Wang, F. Chen, J. Zhao, T. Xie, C. Jiang, H. An, G. Zeng, X. Li, Effective adsorption/electrocatalytic degradation of perchlorate using Pd/Pt supported on N-doped activated carbon fiber cathode, J. Hazard. Mater. 323 (2017) 602–610.
- [14] L. Qu, Z. Wang, X. Guo, W. Song, F. Xie, L. He, Z. Shao, B. Yi, Effect of electrode Pt-loading and cathode flow-field plate type on the degradation of PEMFC, J. Energy Chem. 35 (2019) 95–103.

- [15] H. Olvera-Vargas, C. Trellu, P.V. Nidheesh, E. Mousset, S.O. Ganiyu, C.A. Martínez-Huitle, M. Zhou, M.A. Oturan, Challenges and opportunities for large-scale applications of the electro-Fenton process, Water Res. 266 (2024) 122430.
- [16] N.J. Ambegaonkar, N.H. Tahilramani, P. Patel, P. Patel, Advanced treatment techniques for dye-laden wastewater: a hybrid approach of photocatalytic, hydrodynamic cavitation and ozonation, Indian Chem. Eng. (2025) 1–24.
- [17] D. Zhou, L. Chen, J. Li, F. Wu, Transition metal catalyzed sulfite auto-oxidation systems for oxidative decontamination in waters: a state-of-the-art minireview, Chem. Eng. J. 346 (2018) 726-738.
- [18] S. Eslaminejad, R. Rahimi, M. Fayazi, Sepiolite-metal organic framework-iron oxide catalyst for degradation of rhodamine b using Fenton-like process, J. Taiwan Inst. Chem. Eng. 152 (2023) 105181.
- [19] S. Farazmand, M. Fayazi, Single-step solvothermal synthesis of sepiolite-CoFe₂O₄ nanocomposite as a highly efficient heterogeneous catalyst for photo Fenton-like reaction, Mater. Chem. Phys. 312 (2024) 128627.
- [20] Z. Ye, J.A. Padilla, E. Xuriguera, E. Brillas, I. Sires, Magnetic MIL(Fe)-type MOF-derived N-doped nano-ZVI@C rods as heterogeneous catalyst for the electro-Fenton degradation of gemfibrozil in a complex aqueous matrix, Appl. Catal. B 266 (2020) 118604.
- [21] M. Fayazi, M. Ghanei-Motlagh, Electrochemical mineralization of methylene blue dye using electro-Fenton oxidation catalyzed by a novel sepiolite/pyrite nanocomposite, Int. J. Environ. Sci. Technol. 17 (2020) 4541–4548.
- [22] J. Li, G. Doubek, L. McMillon-Brown, A.D. Taylor, Recent advances in metallic glass nanostructures: synthesis strategies and electrocatalytic applications, Adv. Mater. 31 (2019) 1802120.
- [23] Z. Xie, P. Ye, J. Lv, Y. Deng, W. Liu, Z. Song, Y. Yang, X. Cai, D. Liu, J. Shen, A scalable slurry process to fabricate CuZr amorphous alloy with hybrid lithiophilic oxides for lithium metal anode, J. Alloy. Compd. 965 (2023) 171326.
- [24] L. Chen, X. Jian, P. Zhang, H.-B. Ke, H.-J. Lin, Low-Pt-loaded Pt-CuW metallic glass as highly efficient catalysts for hydrogen evolution reaction, J. Alloy. Compd. 1011 (2025) 178445.
- [25] H.X. Li, Z.C. Lu, S.L. Wang, Y. Wu, Z.P. Lu, Fe-based bulk metallic glasses: glass formation, fabrication, properties and applications, Prog. Mater. Sci. 103 (2019) 235–318
- [26] S. Lu, M. Wang, Z. Zhao, Recent advances and future developments in Fe-based amorphous soft magnetic composites, J. NonCryst. Solids 616 (2023) 122440.
- [27] A.J. dos Santos, M.S. Kronka, G.V. Fortunato, M.R.V. Lanza, Recent advances in electrochemical water technologies for the treatment of antibiotics: a short review, Curr. Opin. Electrochem. 26 (2021) 100674.
- [28] Y. Zhou, Z. Tang, X. Zhao, F. Wu, F. Xie, T. Zhao, C. Da, J. Liu, X. Yang, J. Li, Y. Liu, Enhanced degradation of ofloxacin by novel zero-valent iron particles@V2C MXene composites with efficient activation of peroxomonosulfate: mechanistic insights and DFT calculations, Chem. Eng. J. 504 (2025) 158893.
- [29] J. Luo, L. Wu, D. Liu, Y. Chen, Q. Lv, H. Deng, Preparation of S-scheme heterojunction photocatalyst Y₂O₃/BiOCl and visible light degradation of ofloxacin: photocatalytic mechanism, DFT calculation, degradation pathway, and toxicity evaluation, J. Alloy. Compd. 1010 (2025) 177888.
- [30] Q. Chen, Z. Qi, Y. Feng, H. Liu, Z. Wang, L. Zhang, W. Wang, Nanostructured metallic glass contributing to efficient catalytic degradation of dye wastewater, J. NonCryst. Solids 598 (2022) 121952.
- [31] M.E. Pacheco, L. Bruzzone, Synchronous fluorescence spectrometry: conformational investigation or inner filter effect, J. Lumines 137 (2013) 138–142.
- [32] Q. Wang, B. Wang, Y. Ma, S. Xing, Enhanced superoxide radical production for ofloxacin removal via persulfate activation with Cu-Fe oxide, Chem. Eng. J. 354 (2018) 473–480.
- [33] Y. Lu, M. Feng, Y. Wang, Enhancing the heterogeneous electro-Fenton degradation of methylene blue using sludge-derived biochar-loaded nano zero-valent iron, J. Water Process. Eng. 59 (2024) 104980.
- [34] E. Brillas, C.A. Martínez-Huitle, Decontamination of wastewaters containing synthetic organic dyes by electrochemical methods. An updated review, Appl. Catal. B 166-167 (2015) 603–643.
- [35] A. Xu, X. Sun, S. Fan, Z. Yang, Q. Zhang, Y. Zhang, Y. Zhang, Bio-FeMnOx integrated carbonaceous gas-diffusion cathode for the efficient degradation of ofloxacin by heterogeneous electro-Fenton process, Sep. Purif. Technol. 312 (2023) 123348
- [36] Z. Cao, L. Fan, J. Zhang, P. Yan, H. Wang, W. Dong, Degradation of ofloxacin in electro-Fenton system with adsorption and Green self-regeneration function, J. Water Process. Eng. 48 (2022) 102902.
- [37] R. Patidar, V.C. Srivastava, Mechanistic insight into ultrasound-induced enhancement of electrochemical oxidation of ofloxacin: Multi-response optimization and cost analysis, Chemosphere 257 (2020).
- [38] D. Xu, H. Ma, Degradation of rhodamine b in water by ultrasound-assisted TiO₂ photocatalysis, J. Clean. Prod. 313 (2021) 127758.
- [39] Z. Ai, J. Li, L. Zhang, S. Lee, Rapid decolorization of azo dyes in aqueous solution by an ultrasound-assisted electrocatalytic oxidation process, Ultrason. Sonochem. 17 (2010) 370–375.
- [40] X. Li, X. Jia, C. Zhang, X. Jiang, F. Jiang, Y. Hu, Z. Liu, Z. Liu, A comprehensive overview of advances in heterogeneous Electro-Fenton processes for effective water treatment, Sep. Purif. Technol. 361 (2025) 131470.
- [41] F.C. Moreira, R.A.R. Boaventura, E. Brillas, V.J.P. Vilar, Electrochemical advanced oxidation processes: a review on their application to synthetic and real wastewaters, Appl. Catal. B 202 (2017) 217–261.
- [42] H. Wang, C. Tang, L. Wang, Z. Sun, X. Hu, MOF-derived Co/Fe@NPC-500 with large amounts of low-valent metals as an electro-Fenton cathode for efficient degradation of ceftazidime, Appl. Catal. B 333 (2023) 122755.

- [43] L. Cui, Z. Li, Q. Li, M. Chen, W. Jing, X. Gu, Cu/CuFe₂O₄ integrated graphite felt as a stable bifunctional cathode for high-performance heterogeneous electro-Fenton oxidation, Chem. Eng. J. 420 (2021) 127666.
- [44] Y. Tong, X. Wang, Y. Zhang, J. Xu, C. Sun, Reactive species in peracetic acid-based AOPs: a critical review of their formation mechanisms, identification methods and oxidation performances, Water Res. 272 (2025) 122917.
- [45] J. Song, W. Liu, Z. Xiong, B. Lai, R. Huang, Understanding the multiple functions of the electrolyte tetrapolyphosphate in Electro-Fenton system for effective removal of diclofenac, Sep. Purif. Technol. 330 (2024) 125327.
- [46] P. Duan, X. Yang, G. Huang, J. Wei, Z. Sun, X. Hu, La₂O₃-CuO₂/CNTs electrode with excellent electrocatalytic oxidation ability for ceftazidime removal from aqueous solution, Colloid Surf. A 569 (2019) 119–128.
- [47] J. Hoigné, H. Bader, The role of hydroxyl radical reactions in ozonation processes in aqueous solutions, Water Res. 10 (1976) 377–386.
- [48] S. Chen, M. Cai, Y. Liu, L. Zhang, L. Feng, Effects of water matrices on the degradation of naproxen by reactive radicals in the UV/peracetic acid process, Water Res. 150 (2019) 153–161.
- [49] C. Miège, J.M. Choubert, L. Ribeiro, M. Eusèbe, M. Coquery, Fate of pharmaceuticals and personal care products in wastewater treatment plants – conception of a database and first results, Environ. Pollut. 157 (2009) 1721–1726.
- [50] C. Annabi, F. Fourcade, I. Soutrel, F. Geneste, D. Floner, N. Bellakhal, A. Amrane, Degradation of enoxacin antibiotic by the electro-Fenton process: optimization, biodegradability improvement and degradation mechanism, J. Environ. Manag. 165 (2016) 96–105.
- [51] J. Guan, C. Zhang, H. Shao, H. Jiang, Y. Zhang, H. Xia, L. Zhang, J. Hu, Features of sonochemistry and its application in electrocatalyst synthesis, J. Alloy. Compd. 957 (2023) 170369.
- [52] C. Li, J. Zhang, J. Han, B. Yao, A numerical solution to the effects of surface roughness on water-coal contact angle, Sci. Rep. 11 (2021) 459.
- [53] M. Nosonovsky, B. Bhushan, Superhydrophobic surfaces and emerging applications: Non-adhesion, energy, green engineering, Curr. Opin. Colloid Interface Sci. 14 (2009) 270–280.
- [54] H.L. Li, Z.W. Zhu, S.T. Li, S. Bao, C.M. Liu, S.M. Zhang, H.F. Zhang, Degradation mechanism of acid Orange II in persulfate/Fe-based metallic glass system, J. Phys. Chem. Solids 160 (2022) 110316.

- [55] Y. Li, Y. Liu, Y. Zhan, Y. Zhang, X. Zhao, M. Yang, W. Ruan, Z. Zhang, X. Liang, J. Ma, Peracetic acid-induced nanoengineering of Fe-based metallic glass ribbon in application of efficient drinking water treatment, Appl. Catal. B 355 (2024).
- [56] L. Yang, C. Li, W. Zhai, J. Liu, T. Chen, S. Kou, X. Li, Efficient and sustainable catalytic degradation of methylene blue dye solution by Fe-Si-B amorphous alloy ribbon with large specific surface area, Mater. Today Commun. 43 (2025) 111781.
- [57] J. Xie, C. Zhang, T.D. Waite, Hydroxyl radicals in anodic oxidation systems: generation, identification and quantification, Water Res. 217 (2022) 118425.
- [58] X. Feng, J. Liu, L. Chen, Y. Kong, Z. Zhang, Z. Zhang, D. Wang, W. Liu, S. Li, L. Tong, J. Zhang, Hydrogen Radical-Induced electrocatalytic N2 reduction at a low potential, J. Am. Chem. Soc. 145 (2023) 10259–10267.
- [59] Q. Miao, Z. Cao, Y. Liu, X. Zhou, J. Xie, T. Huo, W. Jiang, Hydrogen radical-driven anthraquinone-promoted H₂O₂ photosynthesis, Chem. Eng. J. 508 (2025) 160957.
- [60] F. Chen, J. Wu, D. Wang, Y. Xia, Q. Song, Y. Liang, P. Wang, B. Chen, Y. Liang, Y. Yin, Y. Wang, M. Song, G. Jiang, Simultaneous generation of hydroxyl and hydrogen radicals from H⁺/OH pairs caused by water-solid contact electrification, Chem. Sci. 15 (2024) 19583–19587.
- [61] A. Babuponnusami, K. Muthukumar, Advanced oxidation of phenol: a comparison between fenton, electro-Fenton, sono-electro-Fenton and photo-electro-Fenton processes, Chem. Eng. J. 183 (2012) 1–9.
- [62] S. Chen, X. Song, X. Song, H. Yan, W. Sun, Photoelectrocatalytic degradation of ofloxacin by ZnO-rGO:N composite material: kinetics, mechanism, and degradation pathways, Mater. Res. Bull. 186 (2025) 113324.
- [63] D. Zhang, R. Zhou, Y. Wu, T. Tan, C. Kong, Z. Yang, T. Wang, H. Zhu, Oxygen vacancy-rich La₂NiO₄ firmly loaded ZIF-67-derived CoC for ofloxacin degradation via enhanced electron transfer and peroxymonosulfate activation, Colloid Surf. A 714 (2025) 136562.
- [64] G. Shao, Q. Wang, F. Miao, J. Li, Y. Li, B. Shen, Improved catalytic efficiency and stability by surface activation in Fe-based amorphous alloys for hydrogen evolution reaction in acidic electrolyte, Electrochim. Acta 390 (2021) 138815.
- [65] Z. Jia, W.C. Zhang, W.M. Wang, D. Habibi, L.C. Zhang, Amorphous Fe₇₈Si₉B₁₃ alloy: an efficient and reusable photo-enhanced Fenton-like catalyst in degradation of cibacron brilliant red 3B-A dye under UV-vis light, Appl. Catal. B 192 (2016) 46–56